Biomedicine & Pharmacotherapy 156 (2022) 113914

Contents lists available at ScienceDirect

Biomedicine & Pharmacotherapy

journal homepage: www.elsevier.com/locate/biopha

A physiologically based pharmacokinetic model for open acid and lactone forms of atorvastatin and metabolites to assess the drug-gene interaction with *SLCO1B1* polymorphisms

Javier Reig-López [a,b], Matilde Merino-Sanjuan [a,b], Alfredo García-Arieta [c], Victor Mangas-Sanjuán [a,b,*]

[a] Department of Pharmacy and Pharmaceutical Technology and Parasitology, University of Valencia. Valencia, Spain
[b] Interuniversity Research Institute for Molecular Recognition and Technological Development, Valencia, Spain
[c] División de Farmacología y Evaluación Clínica, Departamento de Medicamentos de Uso Humano, Agencia Española de Medicamentos y Productos Sanitarios, Calle Campezo 1, Edificio 8, 28022 Madrid, Spain

ARTICLE INFO

Keywords:
Atorvastatin
Lactonization
PBPK
OATP1B1 phenotype
DGI

ABSTRACT

Atorvastatin is the most prescribed 3-hydroxy-3-methylglutaryl coenzyme A reductase inhibitor used to lower cardiovascular risk and constitutes one of the best-selling drugs world-wide. Several physiologically based pharmacokinetic (PBPK) models have been developed to assess its non-straightforward pharmacokinetics (PK) as well as that of its metabolites and have been only applied to assess drug-drug interactions (DDI). Here we present a full PBPK model for atorvastatin and its metabolites able to predict within a 2-fold error their PK after the administration of a solid oral dosage form containing the calcium salt of atorvastatin in single and multiple dosing schedules at 20, 40, and 80 mg and 10 mg dose levels, respectively. Internal validation with data from Phase 1 clinical trials as well as external validation in predicting clinically relevant DDIs consolidated model structure and parameterization. The model has been used to quantitatively assess the drug-gene interaction (DGI) between *SLCO1B1* polymorphisms and atorvastatin exposure and revealed that patients with a reduced activity in hepatic uptake of atorvastatin are at increased risk of suffering muscle discomfort because of a 30% lower clearance ($p < 0.01$), leading to a 40% and 33% higher ($p < 0.05$) atorvastatin AUC and C_{max}, respectively. These findings could explain the reported hazard ratio of 1.4 (95% CI: 1.1–1.7, $p = 0.02$) for suffering statin-induced myopathies and the treatment discontinuation among these patients (odds ratio 1.67, $p = 0.0001$) observed in the context of routine clinical care.

1. Introduction

Atorvastatin (ATS) is one of the most worldwide prescribed 3-hydroxy-3-methylglutaryl-coenzyme A (HMG-CoA) reductase reversible inhibitors for the treatment of hypercholesterolemia and lowering the cardiovascular risk [1]. ATS chemical characteristics [2], as well as pharmacological [3–5], pharmacokinetics (PK) [6,7], and safety and tolerability [8,9], have been extensively reviewed in the last years. Most common side effects are statin-induced myopathies (SIM), which constitute a heterogeneous clinical manifestation such as muscle weakness, muscle pain (myalgia), muscle tenderness, cramps, and arthralgia, with or without an elevation in serum creatine kinase (CK). The most severe form is rhabdomyolysis, a fatal and life-threating adverse effect that occurs in a very low percentage of treated patients (0.1–8.4/100,000 patients-year) [10]. It has been reported that patients with SIM have increased levels of atorvastatin lactone (ATS-L) ($p < 0.01$) and a 2.3-fold prolonged ATS half-life ($t_{1/2}$) ($p < 0.01$), when compared with patients without muscle related side effects [8].

Physiologically-based pharmacokinetic (PBPK) models integrate experimental (in vitro and/or in vivo) information together with a scientifically well-founded mechanistic framework of physiological and biological processes using implicit and explicit assumptions by incorporating drug-, system- and trial design-related parameters [11]. The intended use of PBPK models range from first-in-humans (FIH) dose

* Correspondence to: Department of Pharmacy and Pharmaceutical Technology and Parasitology, University of Valencia, Av Vicent Andrés Estellés, s/n. 46100, Burjassot, Valencia, Spain.
E-mail address: victor.mangas@uv.es (V. Mangas-Sanjuán).

https://doi.org/10.1016/j.biopha.2022.113914
Received 29 July 2022; Received in revised form 17 October 2022; Accepted 24 October 2022
Available online 26 October 2022

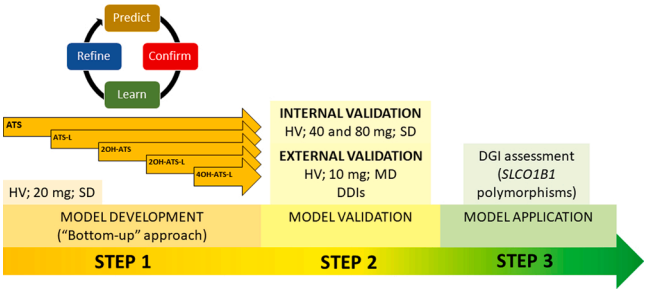

Fig. 1. Workflow for the development of the atorvastatin full PBPK model. HV: healthy volunteers; SD: single dose; MD: multiple dose; DDI: drug-drug interaction; DGI: drug-gene interaction. COLOR online, 2-column width.

selection and assessment of drug-drug interaction (DDI) to dose extrapolation in special populations (paediatrics, pregnancy, obese, ethnicities, etc.), formulation-related, drug product quality attributes, and food effects [12–14]. More recently, the evaluation of drug-gene interactions (DGIs) and drug-drug-gene interactions (DDGIs) has become a new research field and utility of PBPK models [15]. The exponential growth of PBPK models could be related to its mechanistic conceptualization, the prediction of drug concentrations in multiple unobserved physiological compartments and the more reliable implications of the forward projections of *what-if* or experimentally untested scenarios [11,16,17], which has led to a rapid adoption for drug development applications [13,18] and its recognition by the FDA [19, 20] and EMA [21] regulatory authorities.

Recently, several PBPK models of ATS have been published, assessing the PK properties of ATS [22] and its main circulating metabolites 2-hydroxy-atorvastatin (2OH-ATS) and ATS-L [23]. Morse et al. proposed an innovative strategy developing a two-file PBPK model that included ATS and 2OH-ATS (model 1) and ATS-L, ATS, 2-hydrosy-atorvastatin lactone (2OH-ATS-L) and 2OH-ATS (model 2) [24] to account for the time-course of parent and metabolites. However, none of these PBPK models have assessed both ATS-L metabolites (i.e., 2OH-ATS-L and 4-hydroxy-atorvastatin lactone (4OH-ATS-L)) nor considered the administration of a solid oral dosage form to reproduce its solubility-limited absorption, clinical trial design and real-life administration schedules.

The aims of this work are (i) to develop a full PBPK model for ATS and its metabolites in both, open acid and lactone forms able to predict the observed exposure from Phase I clinical trials and (ii) to quantitatively assess the impact of polymorphisms in *SLCO1B1* on ATS exposure.

2. Materials and methods

The ATS PBPK model was developed in the platform Simcyp® Simulator V19 [25] following a "bottom-up" approach and the "predict, confirm, learn and refine" rationale [13]. *In vitro* and in vivo properties of ATS and its metabolites together with the ADME properties of each compound have been extensively characterized in the literature [7], which serve as a scientific basis for the development of the PBPK model. The modelling workflow implemented in the current analysis is depicted in Fig. 1. Firstly, a PBPK model of ATS was developed and its prediction ability was assessed with clinical observations after single oral dose administration of 20 mg ATS [26]. Secondly, we developed the ATS-L, 2OH-ATS, 2OH-ATS-L and 4OH-ATS-L model files sequentially and verified model performance globally in each step with observed clinical data by Riedmaier et al. [26]. As this observed dataset for model development did not include the metabolite 4-hydroxy atorvastatin (4OH-ATS), this compound was not further assessed. A diagram including the description of the metabolic pathways of ATS, ATS-L and their pharmacologically active metabolites can be found elsewhere [7]. Simulations were conducted using the healthy volunteer population file

Table 1
Atorvastatin model file parameters.

Parameter	Value	Source
Physicochemical Properties		
MW (g/mol)	558.64	Drugbank
Compound type	Monoprotic Acid	
logP	5.39	Drugbank
pK_a	4.33	Drugbank
System-Drug Parameters		
f_u	0.022	[24]
B/P	0.61	[29]
Absorption		
Model	ADAM	
P_{app} (Caco-2) (10^{-6} cm/s)	8.6	[32]
Reference compound	Propranolol	[32]
Ref. Comp. P_{app} (10^{-6} cm/s)	20.0	[32]
$P_{eff,man}$	2.046	Simcyp predicted
Formulation	Immediate Release	
Dissolution Type	Dissolution profile	
Absorption Scalars	SI Regional	
Absorption Scalar Duodenum	1.000	Default
Absorption Scalar Jejunum I	1.000	Default
Absorption Scalar Jejunum II	1.000	Default
Absorption Scalar Ileum I	1.000	Default
Absorption Scalar Ileum II	1.000	Default
Absorption Scalar Ileum III	1.000	Default
Absorption Scalar Ileum IV	1.000	Default
Absorption Scalar Colon	0.001	Assumed
Distribution		
Model	Full PBPK	
$V_{d,ss}$ (L/Kg)	2.945	Simcyp Predicted
Prediction Method	2 (Rodgers and Rowland)	
Kp scalar	1.00	Default
Lipid Binding Scalar	10.476	Simcyp Predicted
Transport		
Intestine (efflux)		
P-gp J_{max} (pmol/min)	141.00	[33]
P-gp K_m (μM)	115.00	[33]
System	Caco-2	[33]
RAF/REF	0.99	Default
BCRP CL_{int} (μL/min)	6.00	[22]
Liver (passive difussion) (mL/min/10^6 cells)	0.013	Simcyp Predicted
Drug concentration available	Unbound and unionised	
Liver (active uptake; sinusoidal)		
OATP1B1 CL_{int} (μL/min/10^6 cells)	1011.00	Optimized as explained inSection 2.1
OATP1B3 CL_{int} (μL/min/10^6 cells)	718.00	Optimized as explained inSection 2.1
OATP2B7 CL_{int} (μL/min/10^6 cells)	171.00	Optimized as explained inSection 2.1
Metabolism		
CYP-mediated pathways (Recombinant)		
CYP3A4 V_{max} (pmol/min/pmol) (*ortho*-hydroxylation)	29.30	[34]
CYP3A4 Km (μM) (*ortho*-hydroxylation)	29.70	[34]
System	Baculovirus	
$f_{u,mic}$	1.00	Default
ISEF	0.98	Default
CYP3A4 V_{max} (pmol/min/pmol) (*para*-hydroxylation)	29.80	[34]
CYP3A4 K_m (μM) (*para*-hydroxylation)	25.60	[34]
System	Baculovirus	
$f_{u,mic}$	1.00	Default
ISEF	0.98	Default
CYP3A5 V_{max} (pmol/min/pmol) (*ortho*-hydroxylation)	7.20	[35]
CYP3A5 K_m (μM) (*ortho*-hydroxylation)	54.90	[35]
System	BD SUP	
$f_{u,mic}$	1.00	Default
ISEF	0.24	Default
	10.40	[35]

(*continued on next page*)

Table 1 (*continued*)

Parameter	Value	Source
CYP3A5 V_{max} (pmol/min/pmol) (*para*-hydroxylation)		
CYP3A5 K_m (μM) (*para*-hydroxylation)	42.60	[35]
System	BD SUP	
$f_{u,mic}$	1.00	Default
ISEF	0.24	Default
CYP2C8 V_{max} (pmol/min/pmol) (*para*-hydroxylation)	0.29	[34]
CYP2C8 K_m (μM) (*para*-hydroxylation)	35.90	[34]
System	Baculovirus	
$f_{u,mic}$	1.00	Default
ISEF	0.98	Default
UGT-mediated pathways (Recombinant)		
UGT1A1 V_{max} (pmol/min/mg protein)	120.00	[36]
UGT1A1 K_m (μM)	2.00	[36]
rUGT Scalars (Liver:Intestine: Renal)	1:1:1	Default
UGT1A3 V_{max} (pmol/min/mg protein)	2280.00	[36]
UGT1A1 K_m (μM)	4.00	[36]
rUGT Scalars (Liver:Intestine: Renal)	0.5:1:1	Optimized as explained inSection 2.1
UGT2B7 V_{max} (pmol/min/mg protein)	222.00	[36]
UGT2B7 K_m (μM)	20.00	[36]
rUGT Scalars (Liver:Intestine: Renal)	1:1:1	Default
Excretion		
$CL_{biliary}$ (μL/min/10^6 cells)	50.00	Optimized as explained inSection 2.1
CL_R (L/h)	0.75	[6]

available in Simcyp® Simulator V19. Model performance was assessed by the prediction error ($Parameter_{predicted}$/$Parameter_{observed}$) in exposure PK parameters (AUC and C_{max}). Internal model validation was conducted with clinical data from Phase I studies at 40 and 80 mg dose level after single oral dose administration of the calcium salt form of ATS (ATS-Ca) and external validation was performed using steady-state data after one week of daily administrations of 10 mg ATS-Ca in healthy volunteers. The model was also validated through the simulation of clinically relevant DDIs with known cytochrome P450 (CYP) and organic anion-transporting polypeptides (OATPs) inhibitors that have been observed in vivo. Finally, the full PBPK model was used to investigate the different ATS exposure regarding the activity of OATP1B1 to quantitatively assess the drug-gene interaction (DGI) between *SLCO1B1* polymorphisms and ATS. The development of each model file as well as their validation and application processes are described in more detail below.

2.1. Development of ATS model file

The modelling parameters of the ATS model file are listed in Table 1. The model file represents the immediate release solid oral dosage form of ATS-Ca, which is the actual salt included in the commercially available medicines. *In vitro* ATS-Ca dissolution profiles at pH 1 and 6.8 were incorporated to better account for dissolution in the stomach and small intestine, respectively. The Advanced Dissolution, Absorption and Metabolism (ADAM) model already available in Simcyp® was used and the effective permeability in humans ($P_{eff,man} = 2.046 \cdot 10^{-4}$ cm/s) was predicted from the apparent permeability (P_{app}) determined in Caco-2 cells [27]. Absorption was restricted to the upper part of the gastrointestinal (GI) tract [28], with an extremely low absorption rate at the colon. Efflux processes to the intestinal lumen through breast cancer resistant protein (BCRP) and P-glycoprotein (P-gp), both expressed at the apical side of enterocytes, were also included. A full PBPK distribution model was selected to better assess ATS disposition in vivo. Additionally, the permeability limited liver model was used to account for active uptake through OATPs in hepatocytes, which is known to be the rate determining step for ATS elimination [29]. Sodium-taurocholate transporting polypeptide (NTCP) activity was not included as its contribution to the overall active uptake of ATS has been reported to be negligible when compared to that of OATPs [30].

Table 2
Atorvastatin-lactone model file parameters.

Parameter	Value	Source
Physicochemical Properties		
MW (g/mol)	540.62	Drugbank
Compound type	Neutral	
logP	6.05	[24]
System-Drug Parameters		
f_u	0.012	[24]
B/P	1.00	[24]
Distribution		
Model	Full PBPK	
$V_{d,ss}$ (L/Kg)	129.90	Simcyp Predicted
Prediction Method	2 (Rodgers and Rowland)	
Kp scalar	5.00	Optimized as explained inSection 2.2
Lipid Binding Scalar	0.029	Simcyp Predicted
Metabolism		
CYP-mediated pathways (HLM)		
CYP3A4 V_{max} (pmol/min/mg protein) (*ortho*-hydroxylation)	1397.00	[34]
CYP3A4 K_m (μM) (*ortho*-hydroxylation)	1.60	[34]
$f_{u,mic}$	1.00	Default
CYP3A4 V_{max} (pmol/min/mg protein) (*para*-hydroxylation)	3229.00	[34]
CYP3A4 K_m (μM) (*para*-hydroxylation)	1.80	[34]
$f_{u,mic}$	1.00	Default
ES $t_{1/2}$ (min)	3.00	Optimized as explained inSection 2.2

Elimination was assessed enzymatically, involving different CYPs- and UDP-glucuronosyl transferases (UGT)-mediated pathways. CYP-mediated metabolic reactions of ATS included hydroxylation in position 2 (*ortho*-hydroxylation) and 4 (*para*-hydroxylation). However, only 2OH-ATS was tracked as a metabolite as the model development dataset did not contain information about 4OH-ATS. So, development of the 4OH-ATS compound file was no further performed. Inter System Extrapolation Factors (ISEFs) for CYPs pathways were set depending on the in vitro system where the determinations were performed, with no parameter optimisation at this point and, thus, increasing model identifiability. Recombinant-expressed human UGT (rUGT) scalars were kept with default values with the exception of UGT1A3 in the liver, which was diminished by 50% to best reproduce observed ATS-L $AUC_{0\text{-}inf}$ at 20 mg. Excretion was incorporated into the model mainly through the bile with an optimized biliary clearance (CL_{bile}) of 50 μL/min/10^6 cells to reproduce observed $AUC_{0\text{-}inf}$ at 20 mg. Enterohepatic recirculation was allowed with all the biliary excreted ATS being available for reabsorption, as the extent of ATS absorption from the bile remains unknown [31]. Renal excretion contributed minimally to the systemic clearance with a 2% of the reference value of 37.5 L/h [6].

2.2. Development of ATS-L model file

The ATS-L model file consisted of a refinement of those previously published by Morse et al. [24] and Li et al. [23]. Physicochemical properties were derived from Morse's model. Enzymatic lactonization via UGTs was implemented within the enterocyte to account for the formation of ATS-L from ATS. The distribution process was modelled with a full PBPK model, setting the Kp scalar to 5 to best predict the reported $V_{d,ss}$ value (141.3 L/Kg) [23]. ATS-L elimination was assessed

Table 3
2-hydroxy-atorvastatin model file parameters.

Parameter	Value	Source
Physicochemical Properties		
MW (g/mol)	574.64	[27]
Compound type	Monoprotic Acid	
pK_a	4.33	[27]
logP	5.080	[27]
System-Drug Parameters		
f_u	0.022	Assumed
B/P	0.55	Assumed
Distribution		
Model	Minimal PBPK	
V_{sac} (L/Kg)	0.0032	[27]
SAC k_{in} (1/h)	0.0016	[27]
SAC k_{out} (1/h)	2.78	[27]
$V_{d,ss}$ (L/Kg)	4.036	Simcyp Predicted
Prediction Method	Method 1 (Poulin)	
Kp scalar	1.00	Default
Metabolism		
CYP-mediated pathways (Recombinant)		
CYP3A4 CL_{int} (mL/min/pmol)	3.22	[27]
$f_{u,mic}$	1.00	Default
Additional HLM CL_{int} (μL/min/mg protein)	663.00	[27]
Excretion		
$CL_{biliary}$ (μL/min/10^6 cells)	50.00	Assumed
CL_R (L/h)	0.75	Assumed

enzymatically through CYP3A4 to form the corresponding hydroxylated forms, i.e. 2OH-ATS-L and 4OH-ATS-L. Additionally, lactone hydrolysis in plasma was implemented optimizing the half-life of this process to best predict ATS-L $AUC_{0\text{-inf}}$ at 20 mg. The final value of 3 min of this process agrees with previously published values [24]. Renal excretion of ATS-L was not implemented because of its lower hydrophilicity when comparing to ATS, which already has a minimal renal clearance. Final model parameters are listed in Table 2.

2.3. Development of 2OH-ATS model file

Model parameterisation of 2OH-ATS is shown in Table 3. Regarding red blood cells and plasma protein binding, we assumed the same values than those assigned to ATS, as no direct determination of these parameters has been found in the literature. The distribution model selected was a minimal PBPK model with a single adjusting compartment (SAC) volume (V_{sac}) of 0.0032 L/Kg. CYP3A4-mediated metabolism of 2OH-ATS was implemented, assuming a CL_{int} of 3.22 μL/min/pmol and an unspecific HLM CL_{int} of 663 μL/min/mg protein [27]. Additionally, biliary and renal excretion of this metabolite was incorporated, assuming equal CL_{bile} and CL_R as for ATS, since preclinical information of this metabolite was available [31] and renal excretion is a possible elimination pathway due to its higher hydrophilicity compared to ATS.

2.4. Development of 2OH-ATS-L model file

The physicochemical properties of 2OH-ATS-L were adapted to the values previously published by Morse et al. [24]. A full PBPK model for distribution was selected and a $V_{d,ss}$ of 52 L/Kg was predicted when setting the Kp scalar to 2, to best reproduce 2OH-ATS-L C_{max} at 20 mg dose level. As no CYP-mediated metabolism has been determined for this metabolite, elimination was defined through plasma estherases (assuming equal half-life as for ATS-L) and biliary clearance. 2OH-ATS--glucuronide conjugate is an intermediate reaction product of lactonization as spontaneous cyclization occurs after elimination of the glucuronic moiety [7] and it has been determined in dog bile after oral administration of ATS [31]. For that reason, a CL_{bile} of 10 μL/min/10^6 cells was optimized to best predict its $AUC_{0\text{-inf}}$ at 20 mg dose level. Following the same rationale as with the development of the ATS-L file, no renal clearance was considered for this metabolite. 2OH-ATS-L model file parameters are listed in Table 4.

Table 4
2-hydroxy-atorvastatin-lactone model file parameters.

Parameter	Value	Source
Physicochemical Properties		
MW (g/mol)	556.64	Drugbank
Compound type	Neutral	
logP	6.05	Assumed
System-Drug Parameters		
f_u	0.012	Assumed
B/P	1.00	Assumed
Distribution		
Model	Full PBPK	
$V_{d,ss}$ (L/Kg)	52.002	Simcyp Predicted
Prediction Method	2 (Rodgers and Rowland)	
Kp scalar	2.00	Optimized as explained in Section 2.4
Lipid Binding Scalar	0.029	Simcyp Predicted
Metabolism		
ES $t_{1/2}$ (min)	3.00	Assumed
Excretion		
$CL_{biliary}$ (μL/min/10^6 cells)	10.00	Optimized as explained in Section 2.4

Table 5
4-hydroxy-atorvastatin-lactone model file parameters.

Parameter	Value	Source
Physicochemical Properties		
MW (g/mol)	556.64	Drugbank
Compound type	Neutral	
logP	6.05	Assumed
System-Drug Parameters		
f_u	0.012	Assumed
B/P	1.00	Assumed
Distribution		
Model	Minimal PBPK	
V_{sac} (L/Kg)	10	Optimized as explained in Section 2.5
SAC k_{in} (1/h)	0.0003	Optimized as explained in Section 2.5
SAC k_{out} (1/h)	0.001	Optimized as explained in Section 2.5
$V_{d,ss}$ (L/Kg)	52.002	Simcyp Predicted
Prediction Method	2 (Rodgers and Rowland)	
Kp scalar	2.00	Assumed
Lipid Binding Scalar	0.029	Simcyp Predicted
Metabolism		
ES $t_{1/2}$ (min)	2.00	Optimized as explained in Section 2.5
Additional HLM CL_{int} (μL/min/mg protein)	4000.00	Optimized as explained in Section 2.5
Excretion		
$CL_{biliary}$ (μL/min/10^6 cells)	10.00	Assumed

2.5. Development of 4OH-ATS-L model file

The 4OH-ATS-L model file was developed from 2OH-ATS-L, assuming the same physicochemical properties, plasma protein and red blood cell binding. A minimal PBPK distribution model was selected with V_{sac} of 10 L/Kg and SAC intercompartment clearance (Q) of 1 L/h to best fit the observed data at 20 mg dose level. 4OH-ATS is the less abundant metabolite of ATS and it is mainly formed after ATS-L *para*-hydroxylation through CYP3A4 and subsequent hydrolysis of the hydroxylated lactone. The rate of *para*-hydroxylation of ATS-L is faster than the *ortho*-hydroxylation of ATS-L [7], but systemic exposure to 2OH-ATS is higher. This prompted us to consider a higher elimination rate of 4OH-ATS-L rather than a deeper distribution of the metabolite to

Table 6
Predicted and observed AUC and C_{max} for ATS, ATS-L, 2OH-ATS, 2OH-ATS-L and 4OH-ATS-L in each model development step.

	Analyte	Dose (mg)	Regimen	ObsAUC (ng·h/mL)	PredAUC (ng·h/mL)	Prediction error	ObsC_{max} (ng/mL)	PredC_{max} (ng/mL)	Prediction error
Model development	ATS	20	SD	26.3[a]	34.9[b]	1.33	6.2[c]	5.4[d]	0.87
	ATS-L	20	SD	21.9[a]	19.6[b]	0.89	1.5[c]	2.5[d]	1.67
	2OH-ATS	20	SD	29.8[a]	17.1[b]	0.57	3.9[c]	1.3[d]	0.33
	2OH-ATS-L	20	SD	34.1[a]	37.2[b]	1.01	2.4[c]	1.9[d]	0.79
	4OH-ATS-L	20	SD	7.0[a]	10.1[b]	1.44	0.2[c]	0.2[d]	1.05
Internal validation	ATS	40	SD	50.0[e]	79.0[e]	1.58	14.0 [f]	15.0 [f]	1.07
	2OH-ATS	40	SD	62.0[e]	35.0[e]	0.56	10.0 [f]	3.0 [f]	0.30
	ATS	80	SD	130.0[e]	157.0[e]	1.21	34.0 [f]	29.0 [f]	0.85
	2OH-ATS	80	SD	157.0[e]	82.0[e]	0.52	27.0 [f]	7.0 [f]	0.26
External validation	ATS	10	MD	26.0 [g]	22.5 [g]	0.86	3.5 [h]	4.1 [h]	1.17
	2OH-ATS	10	MD	14.0 [g]	9.0 [g]	0.64	1.1 [h]	0.8 [h]	0.73

[a] $AUC_{0\text{-}inf}$ for the wild type * 1/* 1;
[b] $AU_{C0\text{-}inf}$ for a population representative;
[c] C_{max} for the wild type * 1/* 1;
[d] C_{max} for a population representative;
[e] $AUC_{0–48}$ geometric mean value;
[f] C_{max} geometric mean value;
[g] $AUC_{0–24}$ for the las dose mean value;
[h] C_{max} for the last dose mean value.

other tissues/organs. In this regard, an optimized unspecific HLM CL_{int} of 4000 μL/min/mg protein and a plasma esterases-mediated hydrolysis $t_{1/2}$ of 2 min reproduced the observed $AUC_{0\text{-}inf}$ at 20 mg dose level. Equal biliary clearance as for 2OH-ATS-L and no renal excretion were considered. Parameterisation of 4OH-ATS-L is listed in Table 5.

2.6. Verification of model performance

Single oral dose administration of 20 mg of ATS-Ca to healthy volunteers was tested during model development to assess model accuracy in predicting $AUC_{0\text{-}inf}$ and C_{max} for ATS, ATS-L, 2OH-ATS, 2OH-ATS-L and 4OH-ATS-L. Due to structural limitations of the Simcyp® Simulator, verification of hydroxylated forms of ATS-L (i.e. 2OH-ATS-L and 4OH-ATS-L) were performed independently (two separated, but structurally identical, simulations) as the PBPK platform could only work with one of them as secondary metabolites at a time.

2.7. Internal validation

Single oral dose administration of 40 and 80 mg of ATS-Ca to 500 healthy volunteers (20 trials of 25 individuals each) aged between 20 and 50 years old with a female proportion of 50% was tested to validate the PBPK model developed with clinical observations from Phase I studies. Prediction error in $AUC_{0–48}$ and C_{max} was determined for ATS and 2OH-ATS, and simulated versus observed concentration-time profiles were graphically assessed.

2.8. External validation

2.8.1. Predicting the PK at steady state in healthy volunteers

Multiple oral dose (q.d.) administrations during 1 week of 10 mg ATS-Ca to 18 healthy volunteers aged between 30 and 60 years old with a female proportion of 50% were performed to assess model predictions at steady state conditions. Prediction errors in AUC_{last} and C_{max} were computed and compared with clinical observations [37].

2.8.2. Predicting the outcome of DDI clinical trials

To verify the ability of the PBPK model to predict clinically relevant DDIs, different simulations of administration of ATS-Ca with known CYP (itraconazole and clarithromycin) and OATP (rifampicin at a single dose) inhibitors were performed and compared with clinical observations. **Itraconazole** is a known CYP3A4 inhibitor and both ATS and ATS-L are substrates of CYP3A4. The itraconazole model file already available in Simcyp® Simulator was directly used to perform the simulation in 50 healthy volunteers (5 trials of 10 individuals each). The trial design and subject characteristics were kept consistent with clinical observations reported by Kantola et al. [38]. To assess the impact of ATS-Ca co-administered with **clarithromycin** (CYP3A4 inhibitor) a simulation of 65 healthy volunteers (5 trials of 13 individuals each) was performed to reproduce clinical observations reported by Shin et al. [39], taking the clarithromycin model file directly from the Simcyp® Simulator inhibitors library. Regarding OATP mediated DDI, a simulation of a single dose administration of **rifampicin** (OATP1B1, OATP1B3 and OATO2B1 inhibitor) followed by a single dose of ATS-Ca was simulated in 55 healthy volunteers (5 trials of 11 individuals each), keeping the trial design as well as population characteristics consistent with the paper by Lau et al. [40]. No optimisation of K_i values was performed to run the simulations. Prediction errors in PK exposure parameters, AUC and C_{max}, in the presence and absence of the perpetrator ($PK_{paramInh}/PK_{param}$) were computed.

2.9. Application of the PBPK model to assess DGIs

The PBPK model was ultimately applied to quantitatively evaluate the impact of OATP1B1 activity in ATS exposure, as it has been reported that the *SLCO1B1* genotype influences patients' adherence to ATS therapy as well as increases the risk of SIMs [41]. Since *SLCO1B1* genotyping is not implemented in the Simcyp® Simulator V19, OATP1B1 phenotypes were considered. In this regard, we stratified the ATS exposure for poor (PT), extensive (ET), intermediate (IT) and ultra-rapid (UT) transporters, assuming that the *SLCO1B1 * 5* variant represents a loss-of-function allele that codifies a low OATP1B1 activity (i.e., PT). This analysis was performed through the simulation of a single oral dose administration of 40 mg of ATS-Ca to 500 individuals (20 trials of 25 individuals each) in the internal validation step.

3. Results

Table 6 shows the exposure PK parameters for all the metabolites in both PBPK model development (20 mg dose) and validation (10, 40 and 80 mg dose) steps. Prediction error of AUC and C_{max} of ATS, ATS-L, 2OH-ATS-L and 4OH-ATS-L fell within the 2-fold range in all cases. Simulated concentration-time profiles versus observations for ATS, ATS-L, 2OH-ATS-L and 4OH-ATS-L can be found in the Supplementary

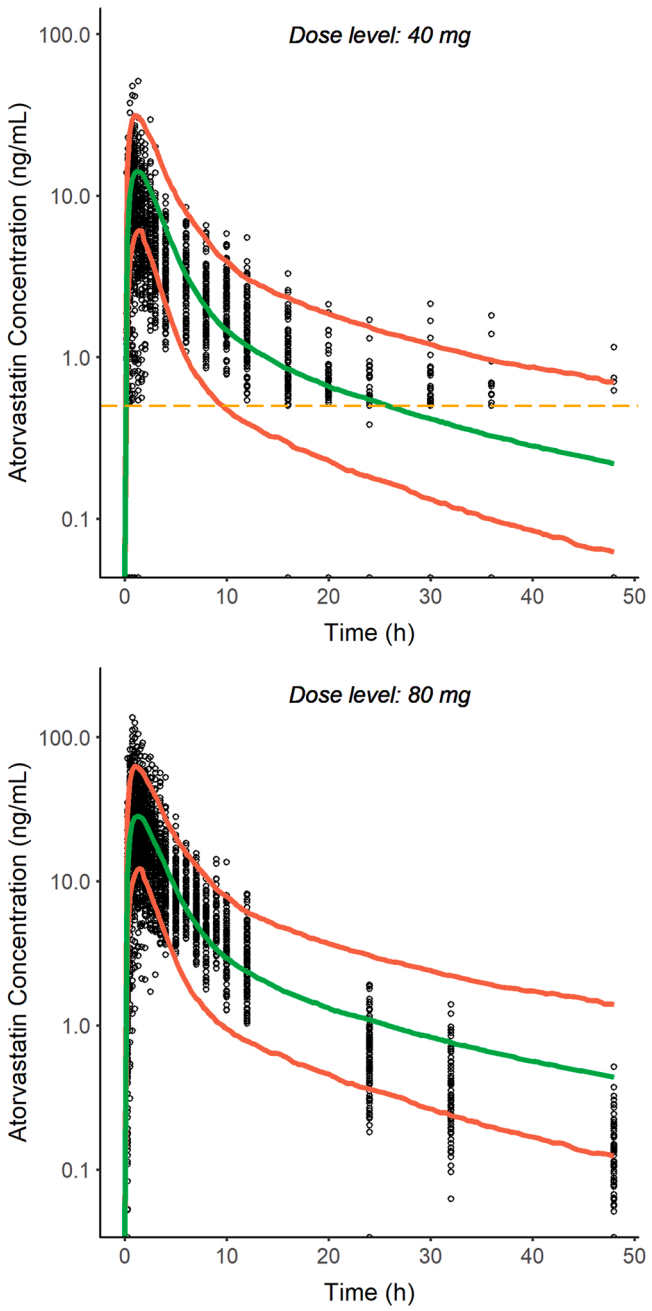

Fig. 2. Plasma concentration-time profiles after the administration of ATS-Ca to healthy volunteers. Green line represents the median profile of all simulated individuals; red lines represent the 5th and 95th percentiles of the simulated individuals; circles represent observed data. The low limit of quantification of ATS was 0.5 ng/mL (orange dotted line). COLOR online, 1-column width.

Material. Additionally, the model was able to properly describe ATS exposure at steady state conditions after the administration of 10 mg q.d. for one week. However, the exposure predictions for 2OH-ATS were lower than those observed after 20, 40 and 80 mg dose administration with mean fold errors of 0.6 for AUC and 0.3 for C_{max}. At steady state conditions, model accuracy in the prediction of 2OH-ATS C_{max} increased up to 0.72, while maintaining the prediction error of 0.6 for AUC.

Fig. 2 shows the simulated mean, 5th and 95th percentiles profiles as well as observed data from Phase I clinical trials at 40 and 80 mg dose levels.

The ATS PBPK model was able to properly describe clinically relevant DDIs with both CYP3A4 and OATPs inhibitors. Table 7 summarizes the observed and predicted ATS and ATS-L AUC and C_{max} ratios as well as the corresponding prediction error According to these results, the mechanisms involved in the metabolic processes linked to CYP3A4 (perturbed by itraconazole and clarithromycin) are adequately characterized for both ATS and ATS-L, since the prediction errors are between 0.66 and 1.45. On the other hand, there is a slight underprediction of ATS exposure in the presence of OATP inhibitors (rifampicin), although the results obtained are within the accepted range (0.61 and 0.79 for AUC and C_{max}, respectively). This outcome demonstrates the validity of the role played by this transporter as an uptake carrier in the elimination of ATS with the current PBPK framework. Simulation details of the DDI trials *in silico* performed, PK profiles of ATS alone and in the presence of these perpetrators and changes in the fraction metabolised through CYP3A4 are reported in the Supplementary Material of this publication.

The impact of OATP1B1 activity on ATS CL, AUC and C_{max} is shown in Table 8. The analysis revealed a statistically significant difference in ATS CL ($p < 0.01$), as PT have a 30% lower clearance than ET individuals. Consequently, ATS AUC and C_{max} are increased by 40% and 33% ($p < 0.05$), respectively, in individuals carrying the *SLCO1B1 * 5* allele. Fig. 3A shows the CL distribution values regarding OATP1B1 activity among the population simulated, showing that patients with lower CL than the CL threshold (414.67 L/h) estimated through a population PK analysis could be at higher risk of suffering muscle discomfort [1]. The clinical impact of OATP1B1 phenotypes on exposure endpoints (AUC and C_{max}) of ATS and ATS-L at 80 mg dose level is depicted in Fig. 3B. The corresponding plots after single dose administration of 10, 20 and 40 mg ATS-Ca are provided in the Supplementary Material.

4. Discussion

The PBPK model here presented can describe within a 2-fold prediction error the exposure metrics, C_{max} and AUC, of ATS and its metabolites ATS-L, 2OH-ATS-L and 4OH-ATS-L, after single dose administration of 20, 40 and 80 mg and multiple administrations of 10 mg of ATS-Ca once daily for one week.

As AUC and C_{max} of ATS increase more than proportionally in the dose range from 0.5 to 80 mg/day [6], these results suggest good model performance, since AUC (1.33, 1.58 and 1.21) and C_{max} (0.87, 1.07 and 0.85) prediction errors at 20, 40 and 80 mg dose levels are randomly distributed within the accepted range (0.5–2).

The PBPK framework was able to characterize ATS-L observed data with prediction errors of 0.89 and 1.67 for AUC and C_{max}, respectively. It has to be noted that lactonization has only been assessed enzymatically through UGTs. Pre-systemic lactonization due to the low pH in the stomach has not been incorporated into the model due to structural limitations of the Simcyp® Simulator, as only one formation pathway can work at a time. For this reason, we did not account for ATS-L absorption in ATS-L model file. Hydroxylated ATS-L metabolites (i.e., 2OH-ATS-L and 4OH-ATS-L) were also well characterized by the model, with prediction errors of 1.01 and 1.44 for AUC and 0.79 and 1.05 for C_{max}, respectively. As they are directly formed after CYP-mediated hydroxylation of ATS-L, these results suggest that considering enzymatic lactonization as the main, but not the only, pathway of ATS-L formation is a good approximation to global ATS PK.

It had been previously suggested that the main formation pathway of hydroxylated metabolites of ATS (i.e., 2OH-ATS and 4OH-ATS) is the ATS lactonization, CYP-mediated hydroxylation and subsequent hydrolysis of the hydroxylated isomers of ATS-L [7]. Direct hydroxylation of ATS would run simultaneously to this metabolic route but playing a minor role in overall ATS elimination. In this sense, we directly used V_{max} values for CYP3A4-, CYP3A5- and CYP2C8-mediated hydroxylation after adjustment with the corresponding ISEF regarding the in vitro system used. It is not surprising, therefore, that exposure to 2OH-ATS is not accurately predicted by our model, with AUC and C_{max} prediction errors of 0.57 and 0.33, respectively, at 20 mg dose level.

Table 7
Predicted versus observed changes in AUC and C_{max} of ATS and ATS-L after concomitant administration of different perpetrators of DDIs.

Perpetrator/Victim	AUC ratio			C_{max} ratio		
	Observed	Predicted	Ratio P/O	Observed	Predicted	Ratio P/O
Itraconazole						
ATS	3.31[a]	2.20[a]	0.66	1.2[b]	1.19[b]	0.99
	3.11[c]	2.08[c]	0.67			
ATS-L	3.98[a]	3.84[a]	0.96	2.26[b]	2.72[b]	1.20
	4.11[c]	3.85[c]	0.94			
Rifampicin						
ATS	7.25[a]	5.74[a]	0.79	10.46[b]	6.35[b]	0.61
Clarithromycin						
ATS	3.08[d]	2.90[d]	0.94	2.16[e]	1.89[e]	0.88
ATS-L	2.67[d]	3.86[d]	1.45	1.5[e]	2.04[e]	1.36

[a] for $AUC_{0\text{-}inf}$ mean values;
[b] for C_{max} mean values;
[c] for $AUC_{0\text{–}72}$ mean values;
[d] for $AUC_{0\text{–}48}$ geometric mean values;
[e] for C_{max} geometric mean values.

Table 8
Comparison of ATS exposure in extensive (ET) and poor (PT) transporters for OATP1B1 activity at 40 mg dose level.

PK param \Phenotype	ET (wild type)	PT (*SLCO1B1*5*)	Fold change[a]	p-value[b]
$AUC_{0\text{–}48}$ (ng·h /mL)	86.77	121.60	1.40	< 0.05
C_{max} (ng/mL)	15.68	20.86	1.33	< 0.05
CL (L/h)	593.47	414.36	0.70	< 0.01
N (%)	304 (60.8)	16 (3.2)	–	–

[a] fold change in $AUC_{0\text{–}48}$, C_{max} and CL was kept at 10, 20 and 80 mg dose levels;
[b] statistical significance in the differences was kept at 10, 20 and 80 mg dose levels. N: number of individuals with the corresponding phenotype.

These results were also observed at higher dose levels in the same magnitude (see Table 6) and differed from those reported by Zhang et al. [27]. However, it must be noted that these authors increased CYP3A4 ISEF up to 7 and CYP2C8 ISEF up to 4 to reproduce the observed 2OH-ATS exposure. In our case, the PBPK model has not been optimized, and the validated ISEFs have been used directly for each CYP isoform.

Successful external validation of the PBPK model with observed data after daily administration of 10 mg ATS-Ca for one week was achieved, with ATS prediction errors of 0.87 and 1.17 for AUC and C_{max}, respectively. To the best of our knowledge, this is the first time that an ATS PBPK model can predict ATS exposure at steady state conditions, thus suggesting good model parameterization and performance. For 2OH-ATS, the PBPK model adequately predicted the exposure in the external validation step, with prediction errors for AUC and C_{max} of 0.64 and 0.72, respectively. The prediction error in AUC at 10 mg after a multiple dose regimen (0.64) is close to the prediction errors obtained after single dose regimen at 20 (0.57), 40 (0.56), and 80 mg (0.52), but the C_{max} prediction after 10 mg ATS daily improved (0.73) compared to single dose regimens (0.33, 0.30, and 0.26), which may be due to a combination of factors: (i) the less sensitivity of C_{max} steady-state observations to detect differences in the absorption process, and (ii) the lower amount of ATS within the enterocyte that favours linear conditions more than at higher dose levels, increasing the lactonization process over CYP-mediated hydroxylation, thus leading to lower C_{max} levels of 2OH-ATS.

As previously mentioned, ATS is a substrate CYP450 [31,35] and special care should be taken during the concomitant administration of substrates and/or inhibitors of this metabolic pathway [42]. Additionally, ATS is also a substrate of the OATPs family [30] and P-gp [33]. In this regard, many efforts had been made to assess the impact of concomitant medications on ATS exposure as a consequence of DDI at metabolic [38,43–45] and/or transporter levels [46–48]. Overall, the model can also predict increases in both, ATS and ATS-L exposures, when co-administered with CYP or OATP inhibitors, thus increasing its performance. Predicted ratios when co-administering ATS with itraconazole or clarithromycin (CYP3A4 inhibitors) suggest that increases in ATS exposure mainly originated from the plasma hydrolysis of the increased levels of circulating ATS-L due to the metabolism inhibition caused by the DDI. This back-conversion to the parent drug has been recommended when modelling ATS [7] and is consistent with the stability of the lactone in plasma [49].

It has been reported that ATS intrinsic uptake clearance is 1900 μL/min/10^6 cells [23] and that the relative contribution to overall uptake clearance is OATP1B1 (52.5%) > OATP1B3 (35%) >> OATP2B1 (8.75%) > NTCP (3.75%) [47]. However, NTCP contribution was negligible when compared to those OATPs. Consequently, OATPs relative contribution was set to 53.2%, 37.8% and 9% for OATP1B1, OATP1B3 and OATP2B1, respectively, with no contribution of NTCP. Good prediction of the DDI between ATS and rifampicin by this model structure justifies the assignment of the relative contribution of each OATP to overall uptake clearance.

The probability of suffering a drug-related adverse event increases as the number of medicines taken by patients does, as inhibition/induction of metabolic routes and/or transport processes can be altered by concomitant medications. Additionally, other factors such as age, renal function, comorbidities, and genetic variation also play a crucial role in the development of adverse effects. In this sense, the presence of polymorphisms in genes codifying transporters or metabolic enzymes involved in drug absorption or disposition processes may represent a relevant area of research in order to explain possible drug-related adverse effects. [50]. PBPK modelling merges system- and drug-related parameters with clinical trial designs, revealing itself as a powerful tool for assessing not only DDIs, but also DGIs [15]. In this work we have applied a full PBPK model of ATS to quantify the impact of different OATP1B1 phenotypes in ATS exposure and confirmed that poor transporter (carrying *SLCO1B1 *5* allele) patients are at higher risk of suffering SIMs due to 30% lower clearance compared to extensive transporter patients, which is in line with the 2.3-fold longer ATS half-life observed in patients suffering SIMs [8]. This result is consistent with the reported hazard ratio of 1.4 (95% CI: 1.1–1.7, $p = 0.02$) for suffering SIMs and could explain the treatment discontinuation among these patients (odds ratio 1.67, $p = 0.0001$) observed in the context of routine clinical care [41]. Additionally, it has been reported that patients with ATS apparent clearance (CL/F) values below 414.67 L/h are at increased risk for suffering muscle discomfort [1] and that the prevalence of mild myalgia among patients taking statins ranges from 0.3% to 33% [10]. Our model predictions reveal that 34.8% of patients have an apparent clearance lower than 414.67 L/h and increased ATS and

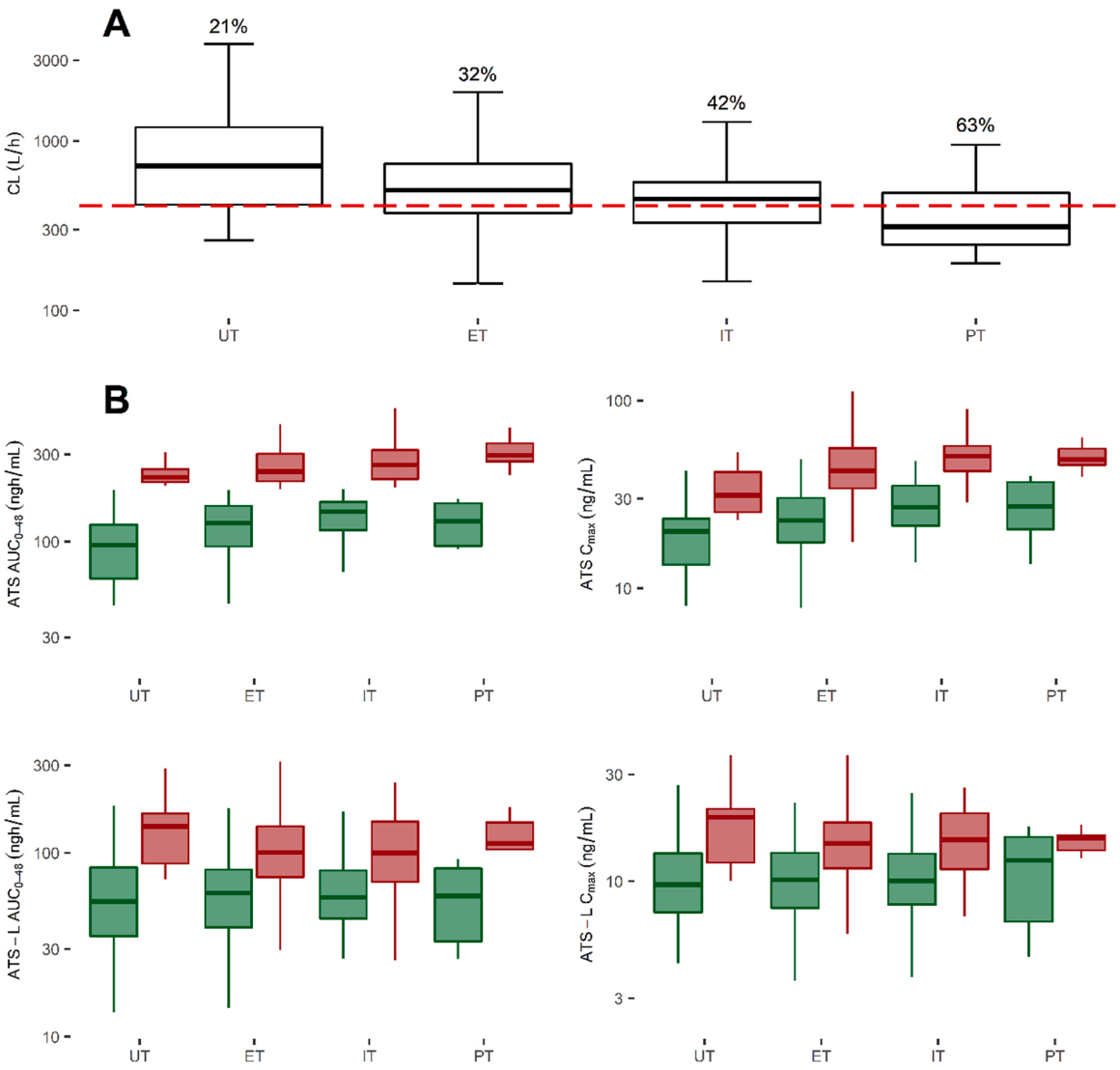

Fig. 3. Clearance, AUC and C_{max} distribution values regarding OATP1B1 phenotype in the simulated population at 80 mg dose level. A: Clearance distribution regarding OATP1B1 phenotype. Red dashed line indicates the CL threshold of 414.67 L/h. The percentage of patients at risk of suffering muscle discomfort is indicated above each box; B: ATS and ATS-L AUC (left plots) and C_{max} (right plots) distribution values regarding OATP1B1 phenotype. Green boxes indicate AUC and C_{max} of patients with ATS CL above 414.67 L/h; red boxes indicate AUC and C_{max} of patients with ATS CL below 414.67 L/h. ET: Extensive transporter; IT: Intermediate transporter; PT: Poor transporter; UT: Ultra-rapid transporter. COLOR online, 2-column width.

ATS-L exposure. Among these patients, the most affected are PT as 63% would be at risk of SIMs and the probability of muscle discomfort would decrease as OATP1B1 activity increases (IT, 42%; ET, 32%; UT, 21%) (Fig. 3 A). In this regard, patients at higher risk of suffering muscle discomfort (CL/F $\leq$ 414.67 L/h) would have 2.2- and 1.76-fold ($p < 0.0001$) higher ATS and ATS-L AUC, respectively (Fig. 3B).

The PBPK model has some limitations that the authors realise and must be mentioned to avoid a misinterpretation of both, model parameterisation and results. In this regard, the PBPK framework does not account for all ATS active metabolites, as 4OH-ATS has not been modelled and 2OH-ATS model predictions are not accurately predicted due to a structural limitation in the PBPK platform, as only one second-generation metabolite can be modelled from the substrate and our proposal is to consider it as a third-generation metabolite mainly formed after the hydrolysis of 2OH-ATS-L. Thus, extending the model to a PBPK/PD structure that could predict the lipid-lowering effect of ATS would not be feasible at the moment. Additionally, the model does not implement pre-systemic lactonization of ATS due to the low pH in the stomach because the Simcyp® Simulator V19 does not allow to track of a metabolite from an endogenous and exogenous pathway at a time. Notwithstanding, our work deepens in mechanistic processes that govern ATS PK, highlights the importance of enzymatic lactonization and predicts a higher probability of suffering muscle discomfort due to an approximately 2-fold increase in ATS and ATS-L exposure. The impact of *SLCO1B1* polymorphisms to predict muscle toxicity is highly dependent on the CL/F threshold considered (414.67 L/h) and, therefore, prospective analyses are encouraged to evaluate the relevance of PK endpoints on muscle toxicity. Clinical evidence would be highly appreciated to externally validate model predicted exposures in *SLCO1B1* polymorphisms after ATS administration.

5. Conclusions

The developed PBPK model was able to mechanistically characterize the exposure metrics of ATS, ATS-L, 2OH-ATS-L and 4OH-ATS-L at different dose levels and after single and multiple dose regimens after oral administration of ATS-Ca. The external validation through the successful prediction of the clinically relevant DDI between ATS and itraconazole, clarithromycin and rifampin endorses the role of the metabolic and transporters pathways here proposed. The model has

been also applied to quantitatively assess the DGI between ATS and *SLCO1B1 * 5*, which originates a 30% decrease in mean ATS clearance when compared to the wild type. As a consequence of this interaction, 63% of patients with the PT phenotype (codified by *SLCO1B1 *5*) could be at a higher risk of suffering muscle discomfort because of an apparent clearance below the previously reported value of 414.67 L/h. Using this cut-off we have been able to mechanistically predict the exposure change to ATS and ATS-L resulting in a 2.2- and 1.76-fold increase in AUC, respectively. Despite more data are needed to validate model predictions in the different phenotypes for OATP1B1, the model here presented can anticipate an exposure-safety relationship between ATS and/or ATS-L and muscle-related adverse events from the mechanistical point of view of physiologically based pharmacokinetics.

Funding Information

This research did not receive any specific grant from funding agencies in the public, commercial, or -not-for-profit sectors.

CRediT authorship contribution statement

Javier Reig-López: Conceptualization, Methodology, Formal analysis, Writing – original draft, Writing – review & editing, Visualization. **Alfredo García-Arieta**: Validation, Resources, Writing – review & editing. **Matilde Merino-Sanjuan**: Validation, Writing – review & editing, Supervision. **Victor Mangas-Sanjuan**: Conceptualization, Validation, Writing – original draft, Writing – review & editing, Visualization, Supervision.

Conflict of interest statement

The authors declare that they have no known competing financial interests or personal relationships that could have appeared to influence the work reported in this paper.

Acknowledgements

The authors want to express their gratitude to Certara UK Limited (Simcyp Division) for granting free access to the Simcyp® Simulator through an academic license agreement (subject to conditions). JRL wants to thank NS for providing language help and writing assistance.

Appendix A. Supporting information

Supplementary data associated with this article can be found in the online version at doi:10.1016/j.biopha.2022.113914.

References

[1] G. Stillemans, A. Paquot, G.G. Muccioli, et al., Atorvastatin population pharmacokinetics in a real-life setting: Influence of genetic polymorphisms and association with clinical response, Clin. Transl. Sci. 15 (2021) 667, https://doi.org/10.1111/cts.13185.
[2] Michael Schachter. Chemical, pharmacokinetic and pharmacodynamic properties of statins: an update. https://doi.org/10.1111/j.1472–8206.2004.00299.x.
[3] H.S. Malhotra, K.L. Goa, Atorvastatin: an updated review of its pharmacological properties and use in dyslipidaemia, Drugs 61 (2001) 1835–1881, https://doi.org/10.2165/00003495-200161120-00012.
[4] C.R. Sirtori, The pharmacology of statins, Pharmacol. Res. 88 (2014) 3–11, https://doi.org/10.1016/j.phrs.2014.03.002.
[5] A. Poli, Atorvastatin: pharmacological characteristics and lipid-lowering effects, Drugs 67 (2007) 3–15, https://doi.org/10.2165/00003495-200767001-00002.
[6] H. Lennernas, Clinical pharmacokinetics of atorvastatin, Clin. Pharmacokinet. 42 (2003) 1141–1160, https://doi.org/42135 [pii].
[7] J. Reig-López, A. García-Arieta, V. Mangas-Sanjuán, M. Merino-Sanjuán, Current evidence, challenges, and opportunities of physiologically based pharmacokinetic models of atorvastatin for decision making, Pharmaceutics 13 (2021) 709, https://doi.org/10.3390/pharmaceutics13050709.
[8] M. Hermann, M. Bogsrud, E. Molden, et al., Exposure of atorvastatin is unchanged but lactone and acid metabolites are increased several-fold in patients with atorvastatin-induced myopathy, Clin. Pharmacol. Ther. 79 (2006) 532–539, https://doi.org/10.1016/j.clpt.2006.02.014.
[9] V.G. Athyros, K. Tziomalos, A. Karagiannis, D.P. Mikhailidis, Atorvastatin: safety and tolerability, Expert Opin. Drug Saf. 9 (2010) 667–674, https://doi.org/10.1517/14740338.2010.495385.
[10] P. du Souich, G. Roederer, R. Dufour, Myotoxicity of statins: mechanism of action, Pharmacol. Ther. (Oxf.) 175 (2017) 1–16, https://doi.org/10.1016/j.pharmthera.2017.02.029.
[11] S. Frechen and A. Rostami-Hodjegan. Quality Assurance of PBPK Modeling Platforms and Guidance on Building, Evaluating, Verifying and Applying PBPK Models Prudently under the Umbrella of Qualification: Why, When, What, How and By Whom? Pharm Res. 1 (123456789) https://doi.org/10.1007/s11095–022-03250-w.
[12] P.J. Kilford, K. Chen, K. Crewe, et al., Prediction of CYP-mediated DDIs involving inhibition: Approaches to address the requirements for system qualification of the Simcyp Simulator, CPT: Pharmacomet. Syst. Pharmacol. 00 (2022) 1, https://doi.org/10.1002/psp4.12794.
[13] M. Shebley, P. Sandhu, A. Emami Riedmaier, et al., Physiologically based pharmacokinetic model qualification and reporting procedures for regulatory submissions: a consortium perspective, Clin. Pharmacol. Ther. 104 (2018) 88–110, https://doi.org/10.1002/cpt.1013.
[14] E. Tsakalozou, K. Alam, A. Babiskin, L. Zhao, Physiologically-Based Pharmacokinetic Modeling to Support Determination of Bioequivalence for Dermatological Drug Products: Scientific and Regulatory Considerations, Clin. Pharmacol. Ther. 111 (2022) 1036–1049, https://doi.org/10.1002/cpt.2356.
[15] J. Wojtyniak, D. Selzer, M. Schwab and T. Lehr. Physiologically Based Precision Dosing Approach for Drug-Drug-Gene Interactions: A Simvastatin Network Analysis. Clin. Pharmacol. Ther. 109 (1201) 201. https://doi.org/10.1002/cpt.2111.
[16] W. Lin, Y. Chen, J.D. Unadkat, X. Zhang, D. Wu, T. Heimbach, Applications, Challenges, and Outlook for PBPK Modeling and Simulation: A Regulatory, Industrial and Academic Perspective, Pharm. Res. 1 (2022), https://doi.org/10.1007/s11095-022-03274-2.
[17] A. Rostami-Hodjegan, Physiologically based pharmacokinetics joined with in vitro-in vivo extrapolation of ADME: a marriage under the arch of systems pharmacology, Clin. Pharmacol. Ther. 92 (2012) 50–61, https://doi.org/10.1038/clpt.2012.65.
[18] E. El-khateeb, S. Burkhill, S. Murby, H. Amirat, A. Rostami-hodjegan, A. Ahmad, Physiological-based pharmacokinetic modeling trends in pharmaceutical drug development over the last 20–years; in-depth analysis of applications, organizations, and platforms, Biopharm. Drug Dispos. 42 (2021) 107, https://doi.org/10.1002/bdd.2257.
[19] Anonymous Physiologically Based Pharmacokinetic Analyses - Format and Content Guidance for Industry. US Official News, 2018.
[20] Anonymous The Use of Physiologically Based Pharmacokinetic Analyses–Biopharmaceutics Applications for Oral Drug Product Development, Manufacturing Changes, and Controls; Draft Guidance for Industry; Availability, Fed. Regist. / FIND 85 (2020) 61953.
[21] Anonymous Guideline on the reporting of physiologically based pharmacokinetic (PBPK) modelling and simulation. European Union News. (2019).
[22] P. Duan, P. Duan, P. Zhao, P. Zhao, L. Zhang, L. Zhang, Physiologically Based Pharmacokinetic (PBPK) Modeling of Pitavastatin and Atorvastatin to Predict Drug-Drug Interactions (DDIs, Eur. J. Drug Metab. Pharm. 42 (2017) 689–705, https://doi.org/10.1007/s13318-016-0383-9.
[23] S. Li, Y. Yu, Z. Jin, et al., Prediction of pharmacokinetic drug-drug interactions causing atorvastatin-induced rhabdomyolysis using physiologically based pharmacokinetic modelling, Biomed. Pharmacother. 119 (2019), 109416, https://doi.org/10.1016/j.biopha.2019.109416.
[24] B.L. Morse, J.J. Alberts, M.M. Posada, et al., Physiologically-Based Pharmacokinetic Modeling of Atorvastatin Incorporating Delayed Gastric Emptying and Acid-to-Lactone Conversion, CPT: Pharmacomet. Syst. Pharmacol. 8 (2019) 664–675, https://doi.org/10.1002/psp4.12447.
[25] U.K. Certara, (Simcyp Division), Simcyp Simula v19 (2020).
[26] S. Riedmaier, K. Klein, U. Hofmann, et al., UDP-Glucuronosyltransferase (UGT) Polymorphisms Affect Atorvastatin Lactonization In Vitro and In Vivo, Clin. Pharm. Ther. 87 (2009) 65, https://doi.org/10.1038/clpt.2009.181.
[27] T. Zhang, Physiologically based pharmacokinetic modeling of disposition and drug–drug interactions for atorvastatin and its metabolites, Eur. J. Pharm. Sci. 77 (2015) 216–229, https://doi.org/10.1016/j.ejps.2015.06.019.
[28] F.N. Khan, M.H.G. Dehghan, Enhanced Bioavailability and Dissolution of Atorvastatin Calcium from Floating Microcapsules using Minimum Additives, Sci. Pharm. 80 (2012) 215–228, https://doi.org/10.3797/scipharm.1104-26.
[29] T. Watanabe, H. Kusuhara, K. Maeda, et al., Investigation of the Rate-Determining Process in the Hepatic Elimination of HMG-CoA Reductase Inhibitors in Rats and Humans, Drug Metab. Dispos. 38 (2010) 215–222, https://doi.org/10.1124/dmd.109.030254.
[30] A. Vildhede, M. Karlgren, E.K. Svedberg, et al., Hepatic uptake of atorvastatin: influence of variability in transporter expression on uptake clearance and drug-drug interactions, Drug Metab. Dispos. 42 (2014) 1210–1218, https://doi.org/10.1124/dmd.113.056309.
[31] Ann E. Black, Roger N. Hayes, Bruce D. Roth, Peter Woo, Thomas F. Woolf, Metabolism and Excretion of Atorvastatin in Rats And Dogs, Drug Metab. Dispos. 27 (1999) 916–923.
[32] J. Li, D.A. Volpe, Y. Wang, et al., Use of Transporter Knockdown Caco-2 Cells to Investigate the In Vitro Efflux of Statin Drugs, Drug Metab. Dispos. 39 (2011) 1196–1202, https://doi.org/10.1124/dmd.111.038075.

[33] X. Wu, L.R. Whitfield, B.H. Stewart, Atorvastatin transport in the Caco-2 cell model: contributions of P-glycoprotein and the proton-monocarboxylic acid co-transporter, Pharm. Res 17 (2000) 209–215, https://doi.org/10.1023/a:1007525616017.
[34] W. Jacobsen, B. Kuhn, A. Soldner, et al., Lactonization Is the Critical First Step in the Disposition of the 3-Hydroxy-3-Methylglutaryl-Coa Reductase Inhibitor Atorvastatin, Drug Metab. Dispos. 28 (2000) 1369–1378.
[35] J.- Park, K.- Kim, S.K. Bae, B.- Moon, K.- Liu, J.- Shin, Contribution of cytochrome P450 3A4 and 3A5 to the metabolism of atorvastatin, Xenobiotica 38 (2008) 1240–1251, https://doi.org/10.1080/00498250802334391.
[36] T.J.J. Schirris, T. Ritschel, A. Bilos, J.A.M. Smeitink, F.G.M. Russel, Statin Lactonization by Uridine 5′-Diphospho-glucuronosyltransferases (UGTs), Mol. Pharm. 12 (2015) 4048–4055, https://doi.org/10.1021/acs.molpharmaceut.5b00474.
[37] M. Hermann, A. Åsberg, H. Christensen, H. Holdaas, A. Hartmann, J.L.E. Reubsaet, Substantially elevated levels of atorvastatin and metabolites in cyclosporine-treated renal transplant recipients (https://doi.org/), Clin. Pharmacol. Ther. 76 (2004) 388–391, https://doi.org/10.1016/j.clpt.2004.07.008.
[38] T. Kantola, K.T. Kivistö, P.J. Neuvonen, Effect of itraconazole on the pharmacokinetics of atorvastatin, Clin. Pharmacol. Ther. 64 (1998) 58–65, https://doi.org/10.1016/S0009-9236(98)90023-6.
[39] J. Shin, D.F. Pauly, M.A. Pacanowski, T. Langaee, R.F. Frye, J.A. Johnson, Effect of Cytochrome P450 3A5 Genotype on Atorvastatin Pharmacokinetics and Its Interaction with Clarithromycin, Pharmacotherapy 31 (2011) 942–950, https://doi.org/10.1592/phco.31.10.942.
[40] Y.Y. Lau, Y. Huang, L. Frassetto, L.Z. Benet, Effect of OATP1B Transporter Inhibition on the Pharmacokinetics of Atorvastatin in Healthy Volunteers, Clin. Pharmacol. Ther. 81 (2007) 194–204, https://doi.org/10.1038/sj.clpt.6100038.
[41] D. Voora, J. Baye, A. Mcdermaid, et al., SLCO1B1*5 Allele is Associated with Atorvastatin Discontinuation and Adverse Muscle Symptoms in the Context of Routine Care, Clin. Pharma Ther. (2022), https://doi.org/10.1002/cpt.2527.
[42] M. Igel, T. Sudhop, K. von Bergmann, Metabolism and drug interactions of 3-hydroxy-3-methylglutaryl coenzyme A-reductase inhibitors (statins, Eur. J. Clin. Pharm. 57 (2001) 357–364, https://doi.org/10.1007/s002280100329.
[43] J.J. Lilja, K.T. Kivistö, P.J. Neuvonen, Grapefruit juice increases serum concentrations of atorvastatin and has no effect on pravastatin, Clin. Pharmacol. Ther. 66 (1999) 118–127, https://doi.org/S0009-9236(99)00102-2 [pii].
[44] J. Shin, D.F. Pauly, M.A. Pacanowski, T. Langaee, R.F. Frye, J.A. Johnson, Effect of Cytochrome P450 3A5 Genotype on Atorvastatin Pharmacokinetics and Its Interaction with Clarithromycin, Pharmacotherapy 31 (2011) 942–950, https://doi.org/10.1592/phco.31.10.942.
[45] I.G. Denisov, J.L. Baylon, Y.V. Grinkova, E. Tajkhorshid, S.G. Sligar, Drug–Drug Interactions between Atorvastatin and Dronedarone Mediated by Monomeric CYP3A4, Biochem. (Easton) 57 (2018) 805–816, https://doi.org/10.1021/acs.biochem.7b01012.
[46] R.A. Boyd, R.H. Stern, B.H. Stewart, et al., Atorvastatin coadministration may increase digoxin concentrations by inhibition of intestinal P-glycoprotein-mediated secretion, J. Clin. Pharm. 40 (2000) 91–98, https://doi.org/10.1177/009127000022008612.
[47] A. Vildhede, M. Karlgren, E.K. Svedberg, et al., Hepatic uptake of atorvastatin: influence of variability in transporter expression on uptake clearance and drug-drug interactions, Drug Metab. Dispos. 42 (2014) 1210–1218, https://doi.org/10.1124/dmd.113.056309.
[48] R.M. Turner, V. Fontana, R. FitzGerald, A.P. Morris, M. Pirmohamed, Investigating the clinical factors and comedications associated with circulating levels of atorvastatin and its major metabolites in secondary prevention, Br. J. Clin. Pharmacol. 86 (2020) 62–74, https://doi.org/10.1111/bcp.14133.
[49] S. Pankaj Partani, Manaswita Verma Sanjay Gurule Arshad Khuroo Tausif Monif. Simultaneous quantitation of atorvastatin and its two active metabolites in human plasma by liquid chromatography/ (-) electrospray tandem mass spectrometry, J. Pharm. Anal. 4 (2014) 26–36, https://doi.org/10.1016/j.jpha.2013.09.007.
[50] M.A. Malki, E.R. Pearson, Drug-drug-gene interactions and adverse drug reactions, Pharm. J. 20 (2020) 355–366, https://doi.org/10.1038/s41397-019-0122-0.